A Chandra X-ray census of the interacting binaries in old open clusters - NGC 188

Vats, S.; van den Berg, M.; Wijnands, R.

Link to publication

A *Chandra* X-ray census of the interacting binaries in old open clusters – NGC 188

Smriti Vats [⬤],[1] Maureen van den Berg [⬤][2][★] and Rudy Wijnands[1]

[1]*Anton Pannekoek Institute for Astronomy, University of Amsterdam, Science Park 904, NL-1098 XH Amsterdam, the Netherlands*
[2]*Harvard-Smithsonian Center for Astrophysics, 60 Garden Street, Cambridge, MA 02138, USA*

ABSTRACT

We present a new X-ray study of NGC 188, one of the oldest open clusters known in our Galaxy (7 Gyr). Our observation with the *Chandra X-ray Observatory* is aimed at uncovering the population of close interacting binaries in NGC 188. We detect 84 sources down to a luminosity of $L_X \approx 4 \times 10^{29}$ erg s^{-1} (0.3–7 keV), of which 73 are within the half-mass radius r_h. Of the 60 sources inside r_h with more than 5 counts, we estimate that $\sim$38 are background sources. We detected 55 new sources, and confirmed 29 sources previously detected by *ROSAT* and/or *XMM–Newton*. A total of 13 sources detected are cluster members, and 7 of these are new detections: four active binaries, two blue straggler stars (BSSs), and, surprisingly, an apparently single cluster member on the main sequence (CX 33/WOCS 5639). One of the BSSs detected (CX 84/WOCS 5379) is intriguing as its X-ray luminosity cannot be explained by its currently understood configuration as a BSS/white-dwarf binary in an eccentric orbit of $\sim$120 d. Its X-ray detection, combined with reports of short-period optical variability, suggests the presence of a close binary, which would make this BSS system a hierarchical multiple. We also classify one source as a new cataclysmic-variable candidate; it is identified with a known short-period optical variable, whose membership to NGC 188 is unknown. We have compared the X-ray emissivity of NGC 188 with those of other old Galactic open clusters. Our findings confirm the earlier result that old open clusters have higher X-ray emissivities than other old stellar populations.

Key words: stars: activity – binaries: close – blue stragglers – cataclysmic variables – open clusters and associations: individual (NGC 188) – X-rays: binaries.

1 INTRODUCTION

X-ray production in single late-type stars is powered by a dynamo mechanism in their convective zones, which means that the faster the star rotates, the higher is its X-ray luminosity. According to the Skumanich law (Skumanich 1972), the rotational velocities of single low-mass stars are proportional to the reciprocal of the square root of their age: as stars get older, they tend to slow down due to magnetic braking (Pallavicini 1989), and correspondingly their X-ray emission decreases. Our Sun is one such old star ($\sim$4.5 Gyr) that has an X-ray luminosity of about 10^{26-27} erg s^{-1} (0.1–2.4 keV; Peres et al. 2000). Such X-ray luminosities are nearly undetectable beyond distances of about a kiloparsec with the current generation of X-ray telescopes, not even with the sensitivity of the *Chandra X-ray Observatory*. However, X-ray observations of old (age $\gtrsim$1 Gyr) open clusters have detected a rich population of X-ray sources that are associated with these clusters. Follow-up studies showed

many of these sources to be close binaries of late-type stars that have been spun-up by tidal interaction (Belloni, Verbunt & Schmitt 1993; van den Berg et al. 2004, 2013; Gondoin 2005; Giardino et al. 2008; Gosnell et al. 2012; Vats & van den Berg 2017). Such tidally interacting binaries, also known as active binaries (ABs), can have either two detached stars comprising the binary, or can have a contact or semidetached configuration like W UMa and Algol binaries, respectively. X-ray sources in old clusters can also be accretion-powered, as in the case of cataclysmic variables (CVs), where a white-dwarf primary accretes matter from a late-type main-sequence donor. These CVs are typically found to the blue of the main sequence in the colour–magnitude diagram (CMD) due to the light from the accretion disc or stream, and possibly due to the contribution from the white dwarf itself. There are also some exotic X-ray sources found in old open clusters, like blue straggler stars (BSSs) and sub-subgiants (SSGs), however the origin of the X-ray emission from these sources, as well as the evolutionary status of these stars themselves, is not well understood (e.g. Geller et al. 2017). Old open clusters are very good laboratories to study binaries, such as ABs, CVs, SSGs, and BSSs, as it is possible to obtain cluster

membership information – and therefore age and distance – for a large number of sources with much less effort than for X-ray sources in the Galactic field. Also, the stellar densities of open clusters lie between those of dense globular clusters (GCs; $\gtrsim 10^4 \, M_\odot \, pc^{-3}$) and the solar neighbourhood ($\sim 0.1 \, M_\odot \, pc^{-3}$). Hence, studying old open clusters aids us in understanding the role of stellar density in stellar and binary evolution. Verbunt (2000) found that the old open cluster M 67 has a higher X-ray emissivity than most GCs. Ge et al. (2015) demonstrated the elevated X-ray emissivity of two open clusters, viz. NGC 6791 and M 67, with respect to old stellar populations other than GCs, like dwarf galaxies and the local solar neighbourhood. In Vats & van den Berg (2017), we were further able to improve the statistics when we found that the old open cluster Collinder 261 (Cr 261; age ∼7 Gyr) is also overluminous in X-rays compared to a few dense GCs.

To expand our understanding of open-cluster X-ray sources and the evolution of binaries in different environments, we are undertaking a survey with *Chandra* of old open clusters with ages between 3.5 and 10 Gyr. The observations are designed to reach a limiting luminosity of at least $L_X \approx 10^{30} \, erg \, s^{-1}$ (0.3–7 keV). In this paper, we focus on the binary population of NGC 188, which at an estimated age of ∼7 Gyr (Sarajedini et al. 1999) is one of the oldest open clusters in the Galaxy. It lies at a distance of 1650 ± 50 pc, has half-mass and core radii of $r_h = 8\overset{'}{.}3 \pm 0\overset{'}{.}6$ and $r_c = 4\overset{'}{.}4 \pm 0\overset{'}{.}1$, respectively, and a reddening of $E(B-V) = 0.083$ (Chumak et al. 2010). NGC 188 was first observed in X-rays using the *ROSAT* Position Sensitive Proportional Counter (PSPC) with a flux detection limit of $\sim 10^{-14} \, erg \, cm^{-2} \, s^{-1}$ in the energy range 0.1–2.4 keV (Belloni, Verbunt & Mathieu 1998), equivalent to a luminosity limit of $\sim 4 \times 10^{30} \, erg \, s^{-1}$ for the quoted distance. The cluster was re-observed with *XMM–Newton* as a performance verification object with a luminosity threshold of $\sim 10^{30} \, erg \, s^{-1}$ (0.5–2.0 keV; Gondoin 2005), but the cluster was not centred at the aimpoint during the observation, leading to asymmetric coverage of the cluster. Recent studies by the WIYN Open Cluster Survey (WOCS) have led to significant progress in our knowledge of NGC 188. Membership of the cluster was established using proper-motion studies performed by Platais et al. (2003) and stellar radial-velocity measurements performed by Geller et al. (2008). We use both of these studies for determining cluster membership of the likely and candidate optical counterparts to the *Chandra* sources detected in the study we present here.

NGC 188 hosts one of the best-studied populations of BSSs (e.g. Geller & Mathieu 2011; Gosnell et al. 2014, 2015). BSSs are stars that are bluer and brighter than the main-sequence turnoff point of a coeval population. They were first discovered in the globular cluster M 3 by Sandage (1953), however, our understanding of their formation is still quite poor. There are currently three suggested scenarios for how BSSs are formed – mass transfer in a binary system, merger of two (or more) stars due to a direct collision, and merger of the inner close binary induced by a tertiary companion in a hierarchical triple (see Davies 2015, for a review). Uncovering blue straggler formation scenarios therefore contributes to our understanding of stellar encounters in clusters. Not all BSSs are expected to be sources of X-ray emission. However, if X-rays are observed from a particular BSS this could give away valuable clues to its current configuration (e.g. it may indicate the presence of a close binary in the system) and thereby constrain its past evolution.

In Section 2 we describe the observations and analysis. In Section 3 we explain how we performed the source classification and we present our results. In Section 4 we discuss our findings, and
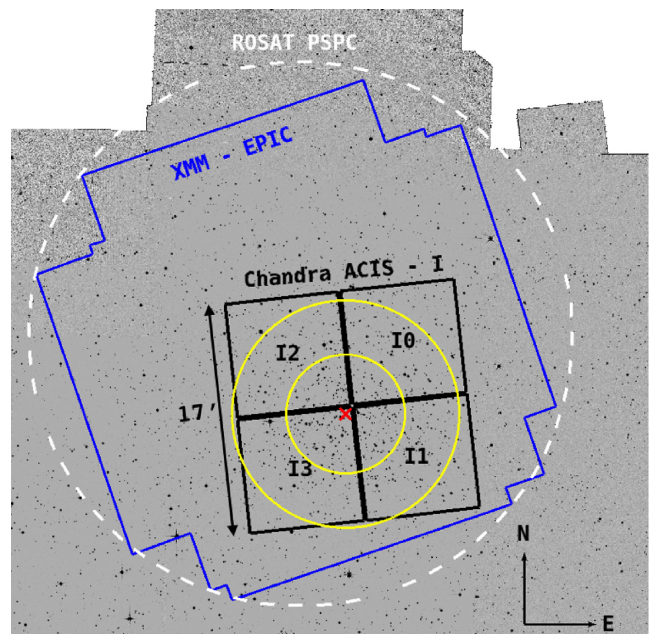

Figure 1. *V*-band image of NGC 188 and its surroundings from Stetson et al. (2004). The white dashed circle shows the central 20 arcmin of the *ROSAT* PSPC observation of NGC 188. The blue composite region shows the area covered by the *XMM–Newton* EPIC-PN and EPIC-MOS detectors. The black squares show the area covered by the *Chandra* ACIS-I chips. The red cross marks the centre of the cluster, and the outer and inner yellow circles mark the half-mass radius, r_h, and the core radius, r_c, respectively.

give details about two particularly interesting sources, including a BSS (WOCS 5379) whose X-ray emission is not well understood. Section 5 is a summary of this work.

2 OBSERVATIONS AND ANALYSIS

2.1 X-ray observations

NGC 188 was observed with the Advanced CCD Imaging Spectrometer (ACIS; Garmire et al. 2003) onboard *Chandra* starting on 2013 July 6 10:25 UTC and the total exposure time of the observation was 24.7 ks (ObsID 14939). The observation was made in very-faint, timed exposure mode, with a single frame exposure time of 3.1 s. The CCDs used were I 0, I 1, I 2, and I 3 from the ACIS-I array, and S 3 from the ACIS-S array. The centre of the cluster ($\alpha_{2000} = 0^h 47^m 12.5^s$, $\delta_{2000} = +85° 14' 49''$; Chumak et al. 2010) was placed close to the *Chandra* aimpoint on the ACIS I 3 chip, so that most of the cluster area within the half-mass radius r_h was imaged on the ACIS-I chips (see Fig. 1 for the chip layout).

We reduced the level-1 event file created by the standard processing pipeline of the *Chandra* X-ray Center using the CIAO 4.5 routines and the CALDB 4.5.5.1 calibration files. We use the `chandra_repro` reprocessing script to obtain the level-2 event file. A background light curve for the energy range 0.3–7 keV was created with the `dmextract` routine in CIAO using source-free areas of the ACIS-I chips, and was analysed with the `lc_sigma_clip` routine. We did not observe any background flares with more than 3σ variations from the average background count rate. Therefore, we used events detected during the entire observation for our further analysis.

2.2 X-ray source detection and source characterization

X-ray source detection and characterization were performed in a similar manner as was done for the cluster Cr 261 by Vats & van den Berg (2017). We summarize the method here. X-ray analysis was performed only on data obtained from chips I 0, I 1, I 2, and I 3, within the energy range of 0.3–7 keV (broad energy band). This energy range was further divided into soft (0.3–2 keV) and hard (2–7 keV) energy bands for our analysis. We did not use data from chip S 3, as S 3 lies far from the aimpoint, leading to large positional errors on sources detected on this chip. These large errors make it difficult to securely identify optical counterparts, and thus to classify the sources.

The CIAO source detection routine `wavdetect` was run for eight wavelet scales ranging from 1.0 to 11.3 pixels, each increasing by a factor of $\sqrt{2}$. Exposure maps were computed for an energy value of 1.5 keV. The `wavdetect` detection threshold (`sigthresh`) was set at 10^{-7}, for which the total number of spurious detections expected is 3.35 for all four ACIS chips and eight wavelet scales combined. For the three energy bands, we detected 72 distinct X-ray sources with more than 2 counts (0.3–7 keV). To check if we had missed any real sources, we ran `wavdetect` again for a more lenient detection threshold of 10^{-6}, and found 84 distinct X-ray sources. The number of spurious detections expected for this threshold for all wavelet scales, over all four chips, is 33.5. One of the 12 extra sources found for the detection threshold of 10^{-6} matches with the known variable V 04 (Hoffmeister 1964), which is a short-period W UMa variable and a plausible X-ray source. We flagged these extra 12 sources, because the majority are likely to be spurious, but have kept them in the master X-ray source list.

For cross-correlating the optical and X-ray catalogues, we calculate the positional uncertainties on the X-ray sources by using the 95 per cent confidence radius on their `wavdetect` positions, P_{err} (Hong et al. 2005). We determined the net source counts using ACIS Extract (AE) (version 2013mar6; Broos et al. 2010) as `wavdetect` is not optimized for this task. All events in the energy range of 0.3–7 keV were extracted. The extraction regions enclose ∼90 per cent of the PSF at 1.5 keV. For sources with five counts or more that spend more than 90 per cent of the total exposure time on the ACIS-I detector (56 sources in total), AE performs variability characterization based on a Kolmogorov–Smirnov (K–S) test on the event arrival times. Based on the K–S variability test, there are 52 sources with no evidence for variability ($0.05 < P_{KS}$); two sources that showed possible variability ($0.005 < P_{KS} < 0.05$; CX 66, CX 75) and two that were definitely variable ($P_{KS} < 0.005$; CX 1, CX 11), where P_{KS} is the probability of having a constant count rate. Neither CX 1 nor CX 11 is a member of NGC 188. The optical counterpart of CX 1 is an optical photometric variable – V 08 (Kaluzny & Shara 1987) – for which a binary origin was considered in Mazur & Kaluzny (1990). We classify CX 11 as a likely background active galactic nucleus (AGN; Section 3.3).

Only two sources in our catalogue (CX 1 and CX 2) have more than 100 net counts (0.3–7 keV) with the brightest source CX 1 having 256 net counts. For most of the other sources, the spectral shape of the X-ray emission is poorly constrained because of the low number of counts detected. We calculated the unabsorbed X-ray fluxes, $F_{X,u}$, using the `Sherpa` package in CIAO. We assumed a 2 keV MeKaL model (`xsmekal`) and a neutral hydrogen column density, $N_H = 5 \times 10^{20}$ cm^{-2} (obtained using the adopted $E(B - V)$ for NGC 188, and the conversion between A_V and N_H given in Predehl & Schmitt 1995), using the `xstbabs` model. A MeKaL model is appropriate for ABs as it describes the emission from a hot, diffuse

gas or optically thin plasma typical for stellar coronae (Güdel 2004). Since we do not know the underlying spectrum of many of our sources, we explored the effect of using different spectral models on the values of $F_{X,u}$. We compared the values of the unabsorbed flux obtained using the 2 keV MeKaL model with those obtained using a 1 keV MeKaL model (`xsmekal`), a 10 keV thermal bremsstrahlung model (`xsbrems`), and a power-law model (`xspowerlaw`) having a photon index $\Gamma = 1.4$. We used the same absorption model and value in all cases (`xstbabs`). The unabsorbed flux values were, on average, about 14 per cent smaller, 26 per cent larger, and 33 per cent larger than the value for the 2 keV MeKaL model, respectively.

We characterize the spectral properties of our X-ray sources using the method of quantile analysis (Hong, Schlegel & Grindlay 2004). In this method, the median energy, E_{50}, and 25 and 75 per cent quantile energies of the event energy distribution (E_{25} and E_{75}, respectively) of a source are used to determine its hardness and spectral shape. For sources with few photon counts, conventional hardness ratios, which use predefined hard and soft energy bands, may not give meaningful results if all those events lie only in either one of the bands. Details of the source properties are presented in Table 1 and the quantile diagrams are shown in Fig. 2.

2.3 Optical source catalogue and X-ray and optical cross-matching

We created an optical master catalogue for NGC 188 by combining the catalogues provided in Platais et al. (2003) and Stetson, McClure & VandenBerg (2004). The positional errors in Platais et al. (2003) are different for each source and are between 1.9 mas and about 100 mas, both in right ascension and declination. The Stetson et al. (2004) catalogue is a combined catalogue from 11 older data sets, leading to different positional errors for different sources. However, they are expected to be less than $0''.1$ in both right ascension and declination. The photometry provided in both catalogues was calibrated on to the standard Johnson BV system. The B and V magnitudes, and the optical coordinates used in our study are obtained from Platais et al. (2003) except for the sources that are only present in Stetson et al. (2004). The range in V magnitude in the Platais et al. (2003) catalogue is $9.0 < V < 22.0$ and in B magnitude it is $9.0 < B < 23.1$.

Despite the fact that *Chandra* sources have good absolute astrometric accuracy,[1] there is still a chance that there is a systematic offset in *Chandra* source positions compared to our optical positions that have been calibrated to the International Celestial Reference System (ICRS), i.e. a boresight, which complicates the search for optical counterparts if not corrected for. To calculate the boresight, we first identified 66 known short-period ($P < 5$ d) variables and one FK Com source among the sources in our optical master catalogue that lie within the *Chandra* field of view (FOV) of NGC 188. Many surveys for optical variables in NGC 188 have been performed, and we have compiled a list of variables from the following references: Kaluzny & Shara (1987), Kafka & Honeycutt (2003), Zhang et al. (2004), and Mochejska et al. (2008). Short-period binaries are expected to be tidally locked, increasing their X-ray activity. FK Com sources are rapidly rotating single stars believed to be the outcome of a binary merger, and this rapid rotation leads to increased X-ray emission. Hence, short-period variables and FK Com stars are likely

---

[1]The 95 per cent confidence radius on absolute positions from *Chandra* ACIS-I is $0''.9$–$1''$ within a distance of 3 arcmin from the aimpoint; see http://cxc.harvard.edu/cal/ASPECT/celmon.

Table 1. Catalogue of *Chandra* sources in NGC 188.

(1) CX	(2) CXOUJ	(3) α (J2000.0) (°)	(4) δ (J2000.0) (°)	(5) Error (arcsec)	(6) θ (arcmin)	(7) $C_{t,net}$	(8) $C_{s,net}$	(9) $F_{X,u}$ (10^{-15} erg cm^{-2} s^{-1})	(10) E_{50} (keV)	(11) Optical match	(12) X	(13) GX
1	005124.1+851803	12.850 489	85.300 911	0.52	6.05	256 ± 16	200 ± 14	123	1.29 ± 0.04	+	26[a]	1
2	005027.5+852211	12.614 557	85.369 736	0.78	8.08	189 ± 13.5	131 ± 12	109	1.50 ± 0.04	+	19	3
3	004244.2+851414	10.684 148	85.237 289	0.63	5.47	74 ± 8.7	72 ± 9	39.1	0.94 ± 0.07	+	30	2
4	004757.0+851456	11.987 457	85.248 873	0.35	1.16	63 ± 8.0	56 ± 8	27.9	1.17 ± 0.07	+	29	–
5	004745.1+852211	11.937 813	85.369 615	0.97	6.97	54 ± 7	29 ± 5	32.3	1.8 ± 0.2	–	20	13
6	004127.6+851636	10.364 926	85.276 781	1.06	7.06	46 ± 6.9	26 ± 5	31.5	1.8 ± 0.2	+	–	4
7	004301.9+851309	10.757 843	85.219 053	0.75	5.44	41 ± 6.5	21 ± 5	21.2	1.9 ± 0.4	+	–	14
8	004448.3+850845	11.201 416	85.145 926	1.13	7.09	40 ± 6	21 ± 5	24.5	2.0 ± 0.2	–	–	40
9	005330.0+852412	13.375 125	85.403 279	3.79	11.90	38 ± 6.6	25 ± 5	46.3	1.4 ± 0.2	–	–	23
10	005112.8+851813	12.803 453	85.303 481	0.90	5.92	35 ± 6	25 ± 5	16.9	1.41 ± 0.19	–	–	1
11	004458.7+851919	11.244 769	85.321 953	0.70	4.80	33 ± 6	20 ± 5	15.5	1.7 ± 0.2	+	–	29
12	004611.4+851444	11.547 483	85.245 451	0.38	1.20	31 ± 6	24 ± 5	13.7	1.47 ± 0.13	+	–	16
13	004522.6+851238	11.344 142	85.210 584	0.53	3.36	30 ± 6	23 ± 5	16.9	1.30 ± 0.13	+	–	18
14	005212.2+851058	13.050 737	85.182 854	1.57	7.73	30 ± 6	16 ± 4	14.7	1.9 ± 0.4	+	–	–
15	004508.8+850859	11.286 548	85.149 710	1.21	6.72	29 ± 6	22 ± 5	14.7	1.50 ± 0.14	+	–	–
16	005247.9+850843	13.199 496	85.145 399	2.82	9.73	27 ± 6	8 ± 3	21.1	2.6 ± 0.2	–	–	–
17	004607.5+851349	11.531 248	85.230 399	0.42	1.85	27 ± 5	21 ± 5	11.8	1.08 ± 0.06	+	–	–
18	004223.8+851515	10.599 279	85.254 186	1.05	5.78	23 ± 5	13 ± 4	13.2	1.8 ± 0.6	–	–	–
19	004056.4+851822	10.235 198	85.306 026	2.04	8.16	23 ± 5	13 ± 4	19.6	2.0 ± 0.3	–	–	46
20	004647.0+851437	11.695 984	85.243 501	0.38	0.73	23 ± 5	19 ± 4	10.0	1.31 ± 0.14	–	–	–
21	004956.3+852113	12.484 570	85.353 716	1.49	6.93	22 ± 5	11 ± 3	12.9	2.1 ± 0.4	–	21	17
22	005002.4+852123	12.510 198	85.356 311	1.58	7.13	22 ± 5	19 ± 5	11.8	1.12 ± 0.09	+	21	17
23	004747.4+851105	11.947 578	85.184 604	0.72	4.28	22 ± 5	10 ± 3	10.9	2.5 ± 0.6	–	–	–
24	005229.8+852315	13.123 994	85.387 501	3.96	10.40	22 ± 5	10 ± 4	14.7	2.4 ± 0.4	+	–	57
25	004256.6+851821	10.735 748	85.305 800	1.15	5.94	21 ± 5	10 ± 3	10.7	2.2 ± 0.5	–	25	36
26	004240.0+851649	10.666 620	85.280 363	1.14	5.65	19 ± 4	16 ± 4	11.2	1.23 ± 0.18	+	–	28
27	004131.7+851814	10.381 958	85.303 937	1.99	7.45	18 ± 5	8 ± 3	10.8	2.4 ± 0.5	–	–	42
28	004415.7+851811	11.065 291	85.302 996	0.86	4.52	17 ± 4	15 ± 4	79.9	1.13 ± 0.13	+	–	31
29	005151.5+852319	12.964 422	85.388 607	4.44	9.97	16 ± 5	9 ± 3	10.1	1.8 ± 0.3	+	–	–
30	004058.6+851859	10.244 231	85.316 497	2.95	8.37	15 ± 4	9 ± 3	10.8	1.96 ± 0.18	–	–	54
31	005107.4+851735	12.781 013	85.293 161	1.26	5.54	15 ± 4	7 ± 3	7.26	2.0 ± 0.6	–	–	–
32	004525.7+852145	11.357 141	85.362 564	1.91	6.79	14 ± 4	7 ± 3	8.60	2.0 ± 0.9	–	–	–
33	005201.6+851739	13.006 512	85.294 043	1.80	6.59	14 ± 4	9 ± 3	7.03	1.5 ± 0.3	+	–	–
34	004540.2+851616	11.417 386	85.270 972	0.49	1.99	14 ± 4	8 ± 3	6.86	2.0 ± 0.5	–	–	–
35	005257.2+851160	13.238 268	85.199 931	2.96	8.05	13 ± 4	9 ± 3	7.21	1.7 ± 0.3	–	–	–
36	004334.4+851429	10.893 236	85.241 471	0.95	4.40	13 ± 4	7 ± 3	6.26	1.9 ± 0.5	–	–	–
37	004752.3+852016	11.968 118	85.337 910	1.19	5.11	13 ± 4	5 ± 2	6.97	2.2 ± 0.4	–	–	–
38	004429.9+852056	11.124 682	85.348 783	1.89	6.48	12 ± 4	12 ± 4	6.26	1.19 ± 0.11	+	–	20
39	004530.0+852329	11.374 944	85.391 295	3.56	8.44	12 ± 4	5 ± 3	8.83	3 ± 1	–	17	–
40	005044.9+851139	12.687 138	85.194 069	1.63	5.86	11 ± 4	9 ± 3	7.38	0.9 ± 0.5	+	–	–
41	004551.2+850922	11.463 303	85.156 187	1.75	6.08	11 ± 4	4 ± 2	5.58	2.9 ± 0.6	–	–	–
42	004507.5+851525	11.281 261	85.256 819	0.58	2.40	11 ± 3	9 ± 3	4.95	1.5 ± 0.3	–	–	25
43	005327.1+851516	13.362 833	85.254 349	3.41	7.94	11 ± 4	7 ± 3	6.36	1.7 ± 0.2	–	–	–
44	005032.7+850824	12.636 064	85.139 905	3.70	8.14	11 ± 4	3 ± 2	5.79	2.8 ± 0.7	–	–	–
45	004224.5+850807	10.602 004	85.135 169	5.46	9.23	10 ± 4	5 ± 3	6.43	1.9 ± 0.7	+	–	–
46	005352.6+851527	13.469 009	85.257 432	4.28	8.46	10 ± 4	3 ± 2	6.45	2.5 ± 0.6	–	–	–
47	004400.1+851534	11.000 257	85.259 436	0.90	3.80	10 ± 3	2 ± 2	5.52	2.5 ± 0.3	–	–	–
48	004736.2+851105	11.900 707	85.184 716	1.04	4.23	10 ± 3	2 ± 2	4.38	4.3 ± 0.7	+	–	–
49	004822.6+851555	12.094 082	85.265 166	0.54	1.76	9 ± 3	9 ± 3	4.34	1.06 ± 0.14	+	–	45
50	004508.0+851313	11.283 363	85.220 383	0.77	3.14	9 ± 3	4 ± 2	5.01	2.3 ± 0.5	–	–	–
51	005245.1+851214	13.187 981	85.203 906	3.86	7.72	9 ± 3	8 ± 3	4.73	0.99 ± 0.07	+	–	–
52	005214.5+851628	13.060 271	85.274 553	2.65	6.54	8 ± 3	6 ± 3	4.01	1.5 ± 0.6	–	–	–
53	004711.7+851332	11.798 637	85.225 445	0.56	1.74	8 ± 3	8 ± 3	3.42	1.0 ± 0.2	+	–	–
54	004511.5+851312	11.297 759	85.219 941	0.81	3.11	8 ± 3	2 ± 2	4.03	2.3 ± 0.9	–	–	–
55	004536.0+851422	11.399 931	85.239 559	0.60	2.02	8 ± 3	4 ± 2	3.50	2 ± 1	–	–	–
56†	004133.8+851231	10.390 686	85.208 479	3.65	7.38	8 ± 3	6 ± 3	5.41	1.2 ± 0.8	+	32	47
57	004340.9+851402	10.920 561	85.233 950	1.24	4.37	8 ± 3	6 ± 3	3.80	1.3 ± 0.6	–	–	–
58	005024.3+851407	12.601 358	85.235 264	1.23	4.32	8 ± 3	3 ± 2	4.20	3.0 ± 0.7	–	–	49
59	005202.4+851429	13.009 953	85.241 512	2.62	6.24	7 ± 3	5 ± 2	3.48	1.4 ± 0.8	–	–	–

Table 1 – *continued*

(1) CX	(2) CXOUJ	(3) α (J2000.0) (°)	(4) δ (J2000.0) (°)	(5) Error (arcsec)	(6) θ (arcmin)	(7) $C_{t,net}$	(8) $C_{s,net}$	(9) $F_{X,u}$ (10^{-15} erg cm^{-2} s^{-1})	(10) E_{50} (keV)	(11) Optical match	(12) X	(13) GX
60	004612.2+851402	11.550 944	85.233 869	0.57	1.62	7 ± 3	7 ± 3	3.08	1.11 ± 0.16	+	–	–
61	005044.4+851739	12.684 838	85.294 036	1.85	5.14	7 ± 3	2 ± 2	3.31	2.3 ± 0.5	–	–	–
62	004506.6+851029	11.277 525	85.174 860	2.05	5.35	6 ± 3	3 ± 2	3.05	3.2 ± 1.0	–	–	–
63	005200.6+851443	13.002 680	85.245 233	2.81	6.18	6 ± 3	3 ± 2	3.11	2.1 ± 0.9	–	–	–
64	004714.2+851408	11.809 200	85.235 518	0.56	1.15	6 ± 3	3 ± 2	2.60	2.6 ± 2.0	–	–	–
65	004704.3+851502	11.767 804	85.250 416	0.51	0.24	6 ± 3	6 ± 3	2.64	1.14 ± 0.13	+	–	–
66†	004240.6+851934	10.669 318	85.326 108	3.90	6.90	6 ± 3	2 ± 2	3.31	3.5 ± 0.8	–	–	–
67	004654.0+851437	11.724 808	85.243 536	0.53	0.68	6 ± 3	5 ± 2	2.62	1.4 ± 0.4	+	–	–
68	004550.0+851257	11.458 336	85.215 886	0.84	2.76	6 ± 3	4 ± 2	2.64	2 ± 1	–	–	–
69†	005028.8+852004	12.620 079	85.334 540	3.47	6.40	6 ± 2	2 ± 2	3.16	2.9 ± 0.9	–	–	–
70†	005011.2+851552	12.546 482	85.264 322	1.42	3.93	5 ± 2	0.	4.46	3.7 ± 0.7	–	–	–
71†	005049.3+851611	12.705 503	85.269 756	2.02	4.76	5 ± 2	5 ± 2	2.37	1.19 ± 0.19	+	–	–
72†	004353.5+851660	10.972 969	85.283 284	1.67	4.28	5 ± 2	3 ± 2	2.52	2.0 ± 0.6	–	–	–
73	004920.7+852017	12.336 173	85.337 920	3.07	5.75	5 ± 2	2 ± 2	2.23	3.6 ± 2.0	–	–	–
74	005138.7+851315	12.911 108	85.220 731	3.48	6.06	5 ± 2	3 ± 2	2.80	1.8 ± 0.5	–	–	–
75	004955.8+851910	12.482 488	85.319 465	2.53	5.27	5 ± 2	5 ± 2	2.34	1.3 ± 0.3	+	–	–
76†	005424.4+850928	13.601 545	85.157 819	19.80	10.90	5 ± 3	6 ± 3	3.24	1.6 ± 0.3	+	–	–
77†	005348.8+851046	13.453 139	85.179 525	13.30	9.57	5 ± 3	7 ± 3	2.77	0.86 ± 0.12	+	–	–
78	004413.9+851633	11.057 838	85.275 946	1.54	3.73	4 ± 2	4 ± 2	1.83	1.11 ± 0.05	+	–	–
79†	004454.0+851841	11.225 075	85.311 377	2.02	4.33	4 ± 2	2 ± 2	1.74	1.5 ± 0.7	–	–	–
80†	004533.1+851343	11.387 968	85.228 607	1.11	2.43	3 ± 2	1 ± 1	1.35	5 ± 1	+	–	–
81	004756.3+851610	11.984 630	85.269 310	0.84	1.42	3 ± 2	1 ± 1	1.64	3 ± 1	–	–	–
82†	004843.3+851203	12.180 331	85.200 703	2.00	3.83	3 ± 2	0.	1.33	6 ± 1	–	–	–
83†	004916.2+851346	12.317 489	85.229 490	1.49	3.13	3 ± 2	3 ± 2	1.30	1.3 ± 0.3	–	–	–
84	005011.2+851439	12.546 689	85.244 166	2.09	3.94	3 ± 2	3 ± 2	1.29	1.17 ± 0.13	+	–	–

Notes.

Col. (1): X-ray catalogue sequence number, sorted by net X-ray counts (0.3–7 keV). Sources that were detected by `wavdetect` using a `sigthresh` of 10^{-6} but not with a `sigthresh` of 10^{-7} have been flagged with †.

Col. (2): IAU designated source name.

Cols. (3) and (4): Right ascension and declination (in decimal degrees) for epoch J2000.0.

Col. (5): 95 per cent confidence radius on `wavdetect` X-ray source position in arcseconds.

Col. (6): Angular offset from the cluster centre ($\alpha_{2000} = 0^h 47^m 12.5^s$, $\delta_{2000} = +85° 14' 49''$; Chumak et al. 2010) in arcminutes.

Col. (7): Net counts extracted in the broad energy band (0.3–7 keV) with 1σ errors.

Col. (8): Net counts extracted in the soft energy band (0.3–2 keV) with 1σ errors.

Col. (9): Unabsorbed X-ray flux in the 0.3–7 keV energy band for a 2 keV MeKaL model and neutral hydrogen column density of 5×10^{20} cm^{-2}.

Col. (10): Median energy E_{50} in keV and 1σ errors on them.

Col. (11) : Information about presence (+) or absence (–) of optical counterpart (details in Table 2).

Col. (12) : ID of *ROSAT* counterpart (Belloni et al. 1998); ^{a} – outside the 95 per cent error circle but within a 4σ match radius.

Col. (13) : ID of *XMM–Newton* counterpart (Gondoin 2005).

X-ray emitters and have lower chances of being spurious matches to X-ray sources (see also Section 2.4). We then cross-matched the ICRS-calibrated optical positions of these variables with our *Chandra* catalogue using a 95 per cent match radius, which is the combination of the error in the optical positions given in the Platais et al. (2003) catalogue scaled to a 95 per cent confidence radius, and the random error on the X-ray positions (P_{err}). Thus, we found 16 counterparts to the X-ray sources which we then used to calculate the boresight. Once an initial boresight was calculated, the cross-matching is repeated and the match radii are augmented with the boresight error. This step was repeated until the net boresight converged. The boresight was found to be $0\overset{''}{.}12 \pm 0\overset{''}{.}11$ in right ascension and $-0\overset{''}{.}14 \pm 0\overset{''}{.}13$ in declination, which is consistent with zero. These values were then added to the old X-ray positions. The method for calculating and correcting for the boresight can be found in more detail in section 3.3.1 of van den Berg et al. (2013).

We matched the boresight-corrected X-ray source list with the optical source list using 95 per cent error radii. Of the 84 unique X-ray sources detected within the FOV, 35 were matched with a single optical counterpart while one source (CX 76) was matched with two optical counterparts. A complete list of candidate counterparts for these 36 X-ray sources can be found in Table 2. Candidate optical counterparts are presented in the CMD of Fig. 3.

On manual inspection of the *V* image provided by Stetson et al. (2004), we find that CX 76 appears to have four more faint optical counterparts, including two that look extended. Of the 48 X-ray sources without any counterparts in the optical catalogue, 12 sources appear to have optical counterparts that were too faint to be reported by Platais et al. (2003) or Stetson et al. (2004). However, we do not report these sources in Table 2 as we do not have photometric information for these faint optical sources.
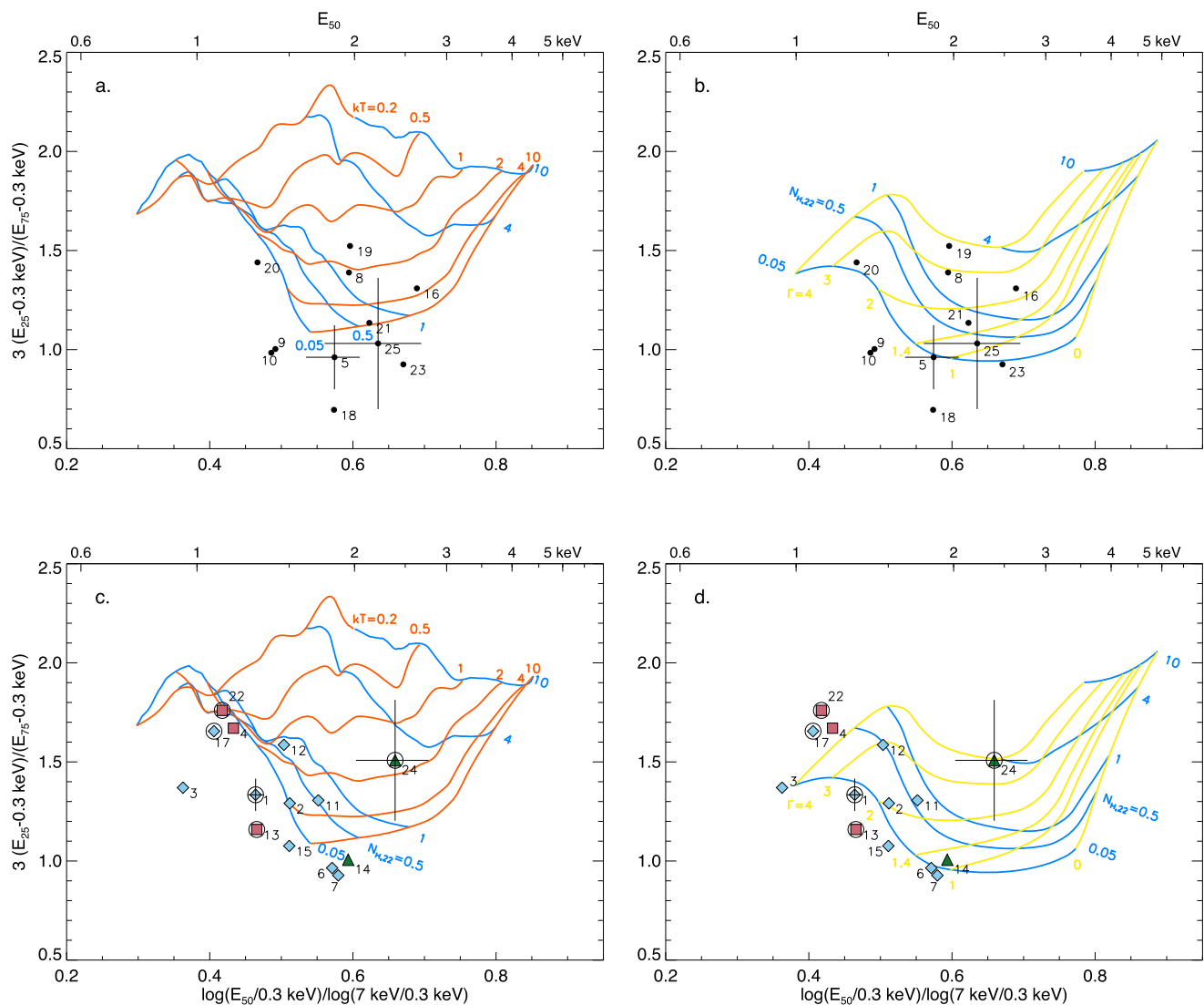
Figure 2. Quantile diagrams with model grids representing a MeKaL plasma (left) and a power-law spectrum (right). The top panels show sources without candidate optical counterparts and the bottom panels show sources with candidate optical counterparts (see Table 2). For a certain choice of model, the plasma temperature (kT) or photon index (Γ), and the column density (N_H) can be estimated from the location of a source inside the grid. The median energy E_{50} can be read off from the top x-axis. Blue lines in all the four quantile diagrams represent different values of N_H normalized in units of 10^{22} ($N_{H,22}$), where $N_{H,22} \approx 0.05$ cm^{-2} is the cluster value. Here we show sources with 20 net counts (0.3–7 keV) or more; error bars are shown only for the sources with the highest and lowest number of counts. In the bottom panels, red squares are members, green triangles have uncertain membership, and blue diamonds are likely non-members. Sources with known periodic photometrically variable counterparts are circled with a larger black open circle.

2.4 False positives test and background galaxies

To estimate the number of spurious matches between our X-ray and optical sources, we calculated the stellar density of optical sources in the cluster field using our optical source catalogue. Inside the core radius r_c as measured by Chumak et al. (2010), the average density is 0.0023 arcsec^{-2}, while in the annulus between r_c and the half-mass radius r_h the average density is 0.001 arcsec^{-2}.

Multiplying the stellar densities with the area covered by the 95 per cent match radii around the X-ray sources within these regions, we expect 0.24 spurious matches among the 13 matches that we find in the central region, and 0.98 spurious matches among the 17 matches in the outer region. We perform the same calculations in order to estimate the number of spurious matches between X-ray sources and photometric variables. The stellar density of variables inside r_c is 0.00012 arcsec^{-2}, while between r_c and r_h the average

density is 5.6×10^{-5} arcsec^{-2}. We expect 0.013 spurious matches among the nine matches that we find in the central region, and 0.040 spurious matches among the six matches that we find in the outer region. Therefore, all matches with short-period variables are likely real.

To estimate the number of background galaxies N_B among the sources in our X-ray catalogue, we used the relation for the cumulative number density of high-galactic-latitude X-ray sources above a given flux limit (equation 5 in Kim et al. 2007). We adopted the ($\log N$)–($\log S$) relation for the *B* band (0.3–8 keV), which is closest to our broad band (0.3–7 keV). To convert counts to fluxes, we assumed a power-law spectrum with $\Gamma = 1.4$. As NGC 188 lies far above the plane of the Galaxy, the integrated Galactic column density in the direction of NGC 188 is the same as the Galactic column density towards the cluster itself (Drimmel, Cabrera-Lavers &

Table 2. Primary *Chandra* catalogue: optical counterpart properties.

(1) CX	(2) OID	(3) Dox (arcsec)	(4) V	(5) B − V	(6) Var	(7) P_{ph} (days)	(8) P_{sp} (days)	(9) MP_{PM}	(10) MP_{RV}	(11) RV variable type	(12) $L_{X,u}$ (10^{30} erg s^{-1})	(13) $\log(F_X/F_V)_u$	(14) Class
Members													
4	5027	0.0521	11.939	1.202	–	–	–	96	98	SM	9.08	−3.44	FK Com
13	4705	0.2194	13.964	0.962	V11	1.2433[z]	35.1780	98	98	BM	5.51	−2.85	AB
22	5258	0.3436	15.569	0.753	V21	1.3836	–	92	–	U	3.84	−2.36	AB
26	4289	0.5519	15.326	0.984	–	–	11.4877	98	98	BM	3.64	−2.48	SSG
33	5639	0.5709	16.038	0.738	–	–	–	90	98	SM	2.29	−2.40	Unc
38	4508	0.8726	16.121	0.751	WV28	0.971 57[k]	–	98	–	BU	2.04	−2.42	AB
40	5459	0.6071	17.518	0.998	V10	3.1596	–	94	–	–	2.41	−1.79	AB
49	4989	0.2781	16.104	0.970	V05	0.5860	–	95	–	–	1.41	−2.58	SSG
53	5078	0.0727	14.465	0.601	V34	4.5295	4.783 03	98	97	BM	1.11	−3.34	BSS
65	5024	0.1649	17.071	0.957	V33	3.2064	–	93	–	–	0.860	−2.41	AB
71	5337	0.8961	15.759	0.848	V04	0.3425	–	96	–	U	0.772	−2.98	AB-WUMa
78	4603	0.5702	17.753	1.140	V37	7.0235	–	91	–	–	0.595	−2.30	AB
84	5379	1.0484	15.372	0.570	WV3	0.181 48[k]	120.2100	98	98	BM	0.421	−3.40	BSS
Uncertain members													
14	5760	1.4338	21.462	0.276	WV2	–	–	–	–	–	4.78	0.09	CV/AGN candidate
24	5569	1.5544	21.865	−0.287	WV2	0.150 59[k]	–	–	–	–	4.79	0.25	CV candidate
28	4566	0.5028	21.904	0.099	–	–	–	–	–	–	2.60	0.00	CV/AGN candidate
29	5565	1.2372	20.979	0.381	–	–	–	–	–	–	3.29	−0.27	CV/AGN candidate
45	4428	1.4499	21.460	0.862	–	–	–	–	–	–	2.09	−0.27	CV/AGN candidate
48	SMV-8056	0.5807	20.721	1.614	–	–	–	–	–	–	1.43	−0.73	Unc
76	7237	1.6723	21.737	0.289	–	–	–	–	–	–	1.06	−0.46	CV/AGN candidate
Non-members													
1	5629	0.0414	13.293	0.800	V08	5.2096[z]	4.086 75	0	0	BN	–	−2.26	Foreground RSCVn
2	5250	0.3049	17.840	0.346	–	–	–	0	–	–	–	−0.49	AGN candidate
3	877-000366	0.9800	9.525	0.678	–	–	–	–	–	–	–	−4.26	Foreground star
6	4035	0.2945	17.776	0.421	–	–	–	0	–	–	–	−1.05	AGN candidate
7	4354	0.2478	20.228	0.407	–	–	–	0	–	–	–	−0.25	AGN candidate
11	4541	0.2566	21.340	0.020	–	–	–	0	–	–	–	0.06	AGN candidate
12	4645	0.1641	21.001	0.233	–	–	–	0	–	–	–	−0.13	AGN candidate
15	4764	0.4219	19.903	0.385	–	–	–	0	–	–	–	−0.53	AGN candidate
17	4679	0.3701	19.182	1.657	WV29	0.974 03[k]	–	0	–	–	–	−0.92	NM
51	5733	0.9698	15.985	0.765	V29	1.1513	8.704 00	98	0	BN	–	−2.59	AB

Table 2 – *continued*

(1) CX	(2) OID	(3) Dox (arcsec)	(4) V	(5) B − V	(6) Var	(7) P_{ph} (days)	(8) P_{sp} (days)	(9) MP_{PM}	(10) MP_{RV}	(11) RV variable type	(12) $L_{X,u}$ (10^{30} erg s^{-1})	(13) log $(F_X/F_V)_u$	(14) Class
56	4082	0.2260	19.336	1.665	–	–	–	0	–	–	–	− 1.20	NM
60	5912	0.2783	16.386	0.831	–	–	–	0	–	–	–	− 2.62	NM
67	5934	0.4161	14.342	0.456	V30	1.2996	–	0	–	BU	–	− 3.51	NM
75	5292	1.5376	13.075	0.545	–	–	–	0	0	SN	–	− 4.06	NM
76	6203	18.5846	15.256	0.524	–	–	–	0	–	–	–	− 3.05	NM
77	6193	1.0664	14.560	0.846	–	–	–	0	–	U	–	− 3.40	NM
80	4681	0.8204	18.330	1.206	–	–	–	0	–	–	–	− 2.20	Unc

Notes.

Col. (1): X-ray catalogue sequence number.

Col. (2): Optical source ID. For CX 48, the optical ID is from the Stetson catalogue (Stetson et al. 2004) as this source was not present in the Platais catalogue (Platais et al. 2003), and for CX 3, the optical ID is from the USNO CCD Astrograph Catalog (UCAC; Zacharias et al. 2013).

Col. (3): Distance between the X-ray source and its optical counterpart in arcsec.

Col. (4): V magnitude.

Col. (5): B − V colour.

Col. (6): Short-period binary counterpart ID (Hoffmeister 1964; Kaluzny & Shara 1987; Kaluzny 1990; Kafka & Honeycutt 2003; Zhang et al. 2004).

Col. (7): Photometric period (in days) of the short-period binary counterpart. Values from Mochejska et al. (2008) unless specified – (^{k}Kafka & Honeycutt 2003; ^{z}Zhang et al. 2004).

Col. (8): Spectroscopic period (in days) of the short-period binary counterpart (Geller et al. 2009).

Col. (9): Membership probability determined from proper-motion studies (Platais et al. 2003).

Col. (10): Membership probability determined from radial-velocity studies (Geller et al. 2008).

Col. (11): Radial-velocity (RV) variable type (Geller et al. 2008); SM – single member, BM – binary member, U – unknown member, BN – binary non-member.

Col. (12): Unabsorbed X-ray luminosity (0.3–7 keV), assuming the source lies at the distance of the cluster (1650 pc).

Col. (13): Unabsorbed X-ray (0.3–7 keV) to optical (V band) flux ratio using a 2 keV MeKaL model and neutral hydrogen column density of 5×10^{20} cm^{-2}.

Col. (14): Object classification: CV – Cataclysmic variable; AB – Active binary; SSG – Sub-subgiant; BSS – Blue straggler star; Unc – Uncertain classification; NM – Single or binary foreground or background (non-member) star; AGN – active galactic nucleus.
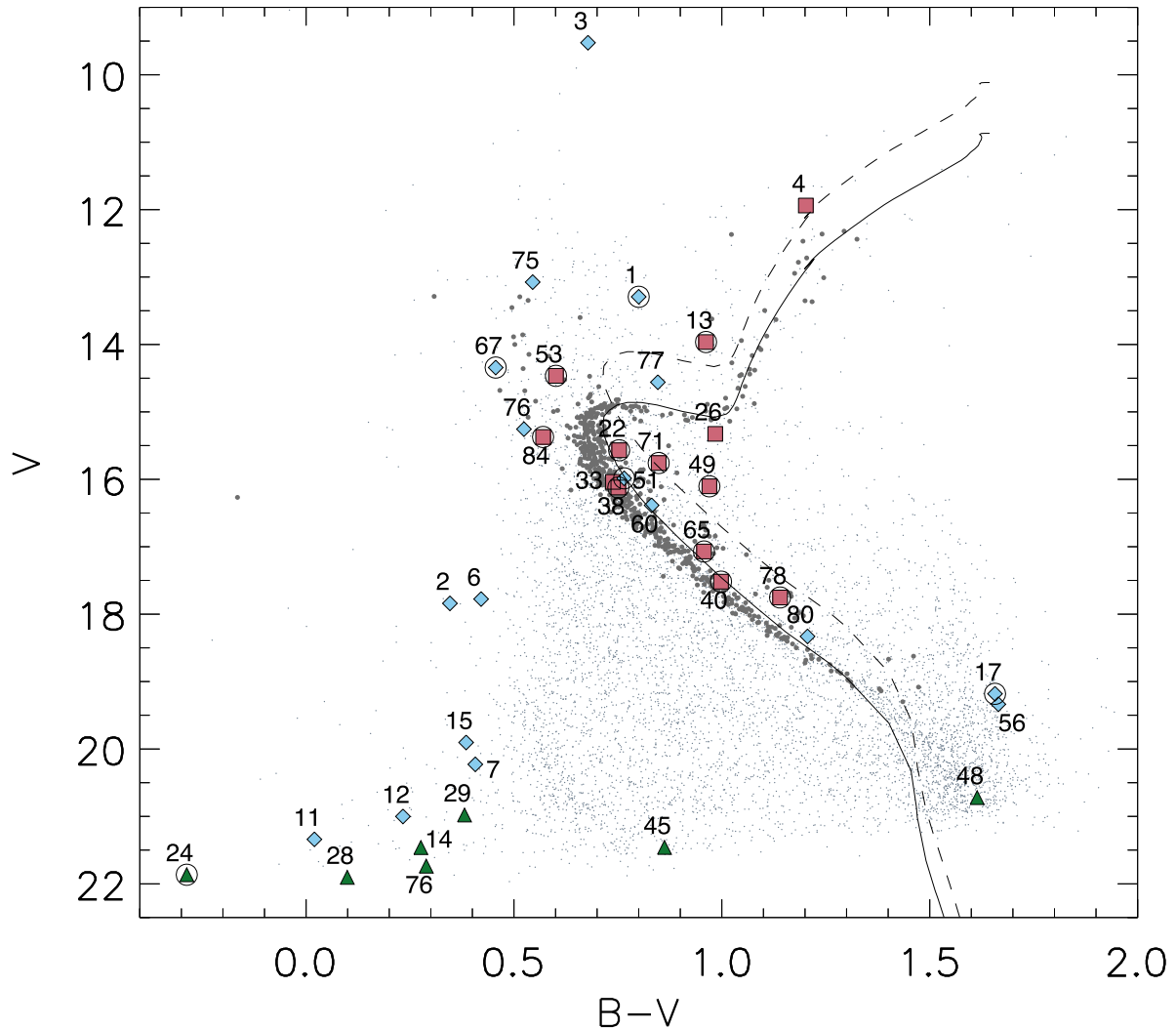
Figure 3. Colour–magnitude diagram of NGC 188. Stars with confirmed membership based on proper motion (MP$_{PM}$ > 90 per cent) are marked with a bold grey dot while the remaining are marked with normal grey dots. Filled colour symbols are candidate optical counterparts to *Chandra* sources. Among them red squares are cluster members, green triangles have uncertain membership, and blue diamonds are likely non-members (MP$_{PM}$ and/or MP$_{RV}$ is 0 per cent). Furthermore, candidate counterparts that are known binary counterparts are circled with a larger black open circle. The solid line represents the isochrone (Bressan et al. 2012; Chen et al. 2014; Tang et al. 2014; Chen et al. 2015) for the reddening associated with the cluster [$E(B - V) = 0.083$]. The dashed line represents the isochrone shifted upwards by −0.75 mag to indicate the limit for photometric main-sequence binaries.

López-Corredoira 2003); therefore, we assume $N_H = N_{H,\text{NGC 188}}$. Closer to the cluster centre, the density of cluster stars is higher and mass segregation makes the radial distribution of binaries more concentrated (Sarajedini et al. 1999; Kafka & Honeycutt 2003; Geller et al. 2008). So we calculated N_B for $r < r_c$, where most X-ray sources that are truly associated with NGC 188 are expected to be. For a detection limit of 5 counts, we expect $N_B \approx 9.3 \pm 3.1$ versus 21 sources actually detected. For a detection limit of 10 counts, it is expected that ∼4.9 ± 2.2 of the eight sources detected within r_c are extragalactic. In the region $r_c < r \leq r_h$, 21.9 ± 4.7 of the 39 sources detected above 5 counts, or 11.3 ± 3.4 of the 29 sources detected above 10 counts are expected to be extragalactic.

2.5 Comparison with other X-ray observations

NGC 188 was previously observed with *ROSAT* (Belloni et al. 1998) with a detection limit of ∼4 × 10^{30} erg s^{-1} (0.1–2.4 keV), and with *XMM–Newton* (Gondoin 2005) with a limit of ∼1 × 10^{30} erg s^{-1}

(0.5–2.0 keV). Both observations were less sensitive compared to our *Chandra* observation in which the faintest detected cluster member has $L_X \approx 4 \times 10^{29}$ erg s^{-1} (0.3–7 keV).[2] We looked for X-ray counterparts to our *Chandra* sources in these two catalogues. Out of the 34 *ROSAT* sources, nine are within the FOV of our *Chandra* observation and one is partially within the FOV. We find that eight sources from the Belloni et al. catalogue (sources labelled with 'X') match with nine of our *Chandra* sources (sources labelled with 'CX') within a 95 per cent match radius (X 19/CX 2, X 20/CX 5 X 30/CX 3, X 29/CX 4, X 21/CX 21+CX 22, X 25/CX 25,　X 17/CX 39,　X 32/CX 56) and one more source matches within an ∼3.6σ match radius (CX 1 matches with X 26 within 6″.8; see Table 1). The 95 per cent match radius is a combination of the 95 per cent error radius on the *Chandra* source position and the 90 per cent error radius on the *ROSAT* source position, scaled

---

[2] All luminosities are normalized to our adopted cluster distance of 1650 pc.

to 95 per cent. However, one source (X 27) in the Belloni et al. catalogue, which lies within the FOV of our *Chandra* observation, has no counterpart(s) in our X-ray catalogue. This is unexpected as the detection limit of the *ROSAT* observation is an order of magnitude higher than that of our *Chandra* observation. It is plausible that X 27 is a variable source in, or projected on to, the cluster. Gondoin (2005) finds 58 sources in NGC 188 of which 31 are within the *Chandra* FOV. In the case of the Gondoin catalogue (sources labelled with 'GX'), errors on source position are not provided, because of which finding cross-matches is not straightforward. However, after recent refinements in the *XMM–Newton* data reduction algorithms, a catalogue of all X-ray sources detected in *XMM–Newton* observations has been compiled by the *XMM–Newton* Survey Science Centre. To find cross-matches between *XMM–Newton* detections and *Chandra* detections, we made use of the sixth data release of the 3XMM *XMM–Newton* serendipitous source catalogue (3XMM-DR6) that contains source detections from all *XMM–Newton* EPIC observations made between 2000 February 3 and 2015 June 4 (Rosen et al. 2016). We find 91 3XMM sources in our *Chandra* FOV (compared to the 31 reported by Gondoin 2005; both source lists for this field are based on the same observations), of which 41 get matched with 40 of the *Chandra* sources within a 95 per cent matching radius (six more 3XMM sources lie within a 3σ radius of another six of the *Chandra* sources). Of these 41 matched sources, only 19 were previously reported by Gondoin (2005); see Table 3.

3 RESULTS

For classifying our X-ray sources, we use three diagnostics, details of which can be found in Vats & van den Berg (2017). In short, we first look at the hardness of the X-ray spectrum, which can be inferred from the position of the source in the quantile diagram (Fig. 2). For sources with fewer than 20 counts, we infer the hardness from the median energy, E_{50}, as the quantile diagram no longer provides reliable information about the underlying spectral shape of sources with few net X-ray counts. As the integrated Galactic N_H is the same as the N_H towards the cluster, Galactic X-ray sources without any intrinsic absorption should not have a N_H larger than the cluster value. Also, coronally active stars and binaries usually have temperatures of about 3–4 keV or less. In the MeKaL grid in Fig. 2, one can see that a combination of these temperatures and N_H constraints gives $E_{50} \lesssim 1.5$ keV. For CVs and AGNs E_{50} may be higher due to their harder intrinsic spectra.

Next, we looked at the ratio of the unabsorbed X-ray flux to optical flux $(F_X/F_V)_u$ for sources with candidate optical counterparts, or the lower limit on this ratio for sources without optical counterparts. We adopted a 2 keV MeKaL model to calculate X-ray fluxes, assuming $N_H = N_{H,\mathrm{NGC\,188}}$ to correct for absorption, and using $V_0 = V - N_{H,\mathrm{NGC\,188}}/(1.79 \times 10^{21})$ (Predehl & Schmitt 1995) for the unabsorbed V magnitude. The calculated flux ratio is overestimated if the adopted N_H is lower than the actual N_H or underestimated if the adopted N_H is higher than the actual N_H. This situation may arise as we do not know the N_H for most sources beforehand. The $\log (F_X/F_V)_u$ ratio also helps us distinguish between coronal and accretion-powered sources. Typically, active stars and binaries have $\log (F_X/F_V)_u \lesssim -1$, while accretion-powered sources have $\log (F_X/F_V)_u \gtrsim -1$ (Stocke et al. 1991).

Finally, for sources with candidate optical counterparts, we also look at the position of these optical sources in the CMD. In most cases, this works reasonably well to separate active stars and binaries from AGNs (which often have blue optical colours and lie far off

Table 3. Cross-reference table between our *Chandra* catalogue and the 3XMM-DR6 catalogue.

CX	SRCID	Flux $(10^{-15}$ erg cm^{-2} s$^{-1})$	GX
3	201006401010002	91 ± 2	2
4	201006401010022	21 ± 1	–
5	201006401010014	16.3 ± 0.7	13
6	201006401010004	29.0 ± 0.9	4
7	201006401010020	24 ± 1	14
8	201006401010048	15 ± 1	40
9	201006401010038	17 ± 1	23
11	201006401010031	8.1 ± 0.5	29
12	201006401010019	15.3 ± 0.8	16
13	201006401010027	15.2 ± 0.8	18
15	201006401010074	11 ± 1	–
17	201006401010047	6.9 ± 0.6	–
18	201006401010075	4.5 ± 0.4	–
19	201006401010041	6.7 ± 0.5	46
24	201006401010063	9.3 ± 0.8	57
25	201006401010045	8.3 ± 0.5	36
26	201006401010034	11.9 ± 0.6	28
27	201006401010033	7.3 ± 0.5	42
29	201006401010101	7.9 ± 0.7	–
30	201006401010053	6.4 ± 0.5	54
34	201006401010162	2.0 ± 0.3	–
35	201006402010183	1.6 ± 0.9	–
36	201006401010066	3.8 ± 0.5	–
37	201006401010093	3.0 ± 0.4	–
38	201006401010026	13.0 ± 0.6	20
39	201006401010084	5.1 ± 0.5	–
45	201006401010133	4 ± 1	–
49	201006401010055	7.1 ± 0.6	45
51	201006402010136	10 ± 2	–
55	201006402010140	2.2 ± 0.5	–
56	201006401010046	15.0 ± 0.8	47
58	201006401010072	6.4 ± 0.7	49
59	201006401010128	5.0 ± 0.8	–
64	201006401010119	3.3 ± 0.5	–
72	201006401010122	2.6 ± 0.3	–
74	201006401010148	2.7 ± 0.6	–
76	201006401010123	9 ± 2	–
76	201006402010151	7 ± 2	–
77	201006401010080	13 ± 2	–
78	201006402010175	1.4 ± 0.4	–
79	201006401010155	2.9 ± 0.5	–

Notes.
Col. (1): *Chandra* ID.
Col. (2): *XMM–Newton* serendipitous source catalogue ID.
Col. (3): Flux obtained from *XMM–Newton* (0.5–4.5 keV)
using a power-law model with $\Gamma = 1.7$ and $N_H = 3 \times 10^{20}$ cm^{-2}.
Col. (4): X-ray source ID from Gondoin (2005).

the stellar main sequence in the CMD) and CVs (which typically are blue, too).

3.1 Cluster members

To classify sources as cluster members or non-members, we considered the membership probabilities of their candidate optical counterparts from both proper-motion studies (MP$_{PM}$; Platais et al. 2003) and radial-velocity studies (MP$_{RV}$; Geller et al. 2008). All optical sources that match with our *Chandra* sources and for which membership information is available fall in two well-separated membership categories. A total of thirteen X-ray sources have optical
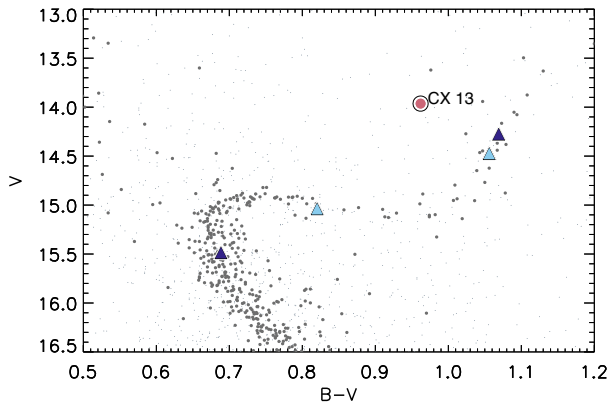
Figure 4. Photometric decomposition of the optical counterpart of CX 13 in to its plausible components. The two light blue triangles represent one pair of plausible binary components and the two dark blue triangles represent another pair.

counterparts with MP_{PM} and/or MP_{RV} larger than 90 per cent; we consider these as probable cluster members. For 16 X-ray sources MP_{PM} and/or MP_{RV} is 0 per cent; these sources are briefly discussed in Section 3.3. In almost all cases, MP_{PM} and MP_{RV} are consistent; the only exception is CX 51 (Section 3.3).

Of the thirteen X-ray sources that are likely members, six had previously been detected by *ROSAT* or *XMM–Newton* or both, and seven are new detections (CX 33, CX 40, CX 53, CX 65, CX 71, CX 78, CX 84). All new detections lie within r_h, with four lying within r_c. In the following subsections, we first discuss the ABs (Section 3.1.1), and then the anomalous stars like BSSs (Section 3.1.2) and an uncertain classification (Section 3.1.3).

3.1.1 Active binaries

For selecting possible ABs in NGC 188, we picked sources with optical counterparts that lie along the cluster main sequence or sub-giant branch in the CMD. We allowed for the possible contribution to the optical light from binary companions. For a binary with two companions of the same mass, the maximum decrease in *V* magnitude is 0.75 and the resulting binary sequence is indicated by the dotted isochrone in Fig. 3. We also considered their X-ray properties, and photometric or radial-velocity periods. Seven *Chandra* sources were thus selected as likely ABs, of which the brightest three were detected before (CX 13/GX 18, CX 22/X 21, CX 38/GX 20). All have E_{50} values $\lesssim 1.5$ keV, $\log F_X/F_V \lesssim -1.8$, and are matched with short-period ($\lesssim 11$ d) photometric or radial-velocity variables. We have classified these sources as ABs in NGC 188, and classify them as 'AB's in column 14 of Table 2.

We add a few notes on individual sources. CX 71 is matched to the W UMa-type contact binary V 04 (Hoffmeister 1964; Mochejska et al. 2008); we confirm its cluster membership using the period–colour relationship for W UMa's (Rucinski 1994). The counterpart to the AB CX 13 (V 11) lies in a region of the CMD that is ~0.15 mag bluer than the red giant branch. As noted by several authors, this location can be explained by a combination of a relatively unevolved red giant and a less-evolved member. We illustrate this in Fig. 4, where we photometrically decompose the optical source in to its plausible binary components, i.e. we investigate the fluxes of different types of stars that can be combined to give a total flux equal to the flux of CX 13. We further discuss this source in Section 4.1. The counterpart to CX 22 (V 21) was classified by Zhang et al. (2004)

as a W UMa binary based on its light curve; with a photometric period of $P_{ph} \approx 1.17$ d, they note it is the longest period W UMa in NGC 188. Mochejska et al. (2008), however, find a period of $P_{ph} \approx 1.38$ d (assuming one maximum/minimum per cycle, instead of two as would be the case for W UMa's) and classify it as a BY Dra system. To be a W UMa, its period would have to be ~2.77 d, which is decisively too large for a W UMa star. We thus adopt the period by Mochejska et al., also because the light curve shown in Zhang et al. (2004) does not show the typical W UMa-type shape.

3.1.2 Blue stragglers, sub-subgiants, and FK Com stars

The two BSSs in NGC 188 detected by *Chandra* are both new X-ray detections. The BSS counterpart of CX 53 (WOCS 5078 or V 34) was first observed as a variable by Mochejska et al. (2008) with a period of ~4.5 d. Geller et al. (2008) found it to be a double-lined spectroscopic binary with a period of ~4.8 d. The orbital period is short enough for strong tidal coupling and enhanced X-ray emission, but interestingly, the orbit is eccentric ($e \approx 0.12$) pointing at a recent dynamical encounter or a third companion (see discussion in Geller et al. 2009). CX 84 (WOCS 5379 or WV 3) is a BSS with a white-dwarf companion (Gosnell et al. 2014). The difference between the reported radial-velocity ($P_{sp} \approx 120$ d; Geller et al. 2009) and photometric ($P_{ph} \approx 0.18$ or 0.36 d; Kafka & Honeycutt 2003) periods is intriguing. We discuss CX 84 in more detail in Section 4.2.

CX 26 (GX 28) and CX 49 (GX 45) are classified as SSGs. This nomenclature arises from their location on the CMD, wherein they lie below the subgiant branch and to the red of the main sequence. Several scenarios have been proposed for how SSGs arrive at their current CMD position (see Geller et al. 2017, and the references within). CX 49 is the variable V 05 discovered by Kaluzny & Shara (1987) with $P_{ph} \approx 0.59$ d. The light curve for V 05 does not appear to have equal maxima and minima, suggesting it may not be a W UMa binary as suggested in Mochejska et al. (2008), but a semidetached binary.

CX 4 (X 29) is a red giant and the brightest cluster member detected in X-rays; it was classified as an FK Com variable by Harris & McClure (1985) and a single cluster member by Geller et al. (2009).

3.1.3 CX 33: uncertain classification

The optical counterpart to the new source CX 33 lies on the cluster main sequence, has a median energy value of $E_{50} \approx 1.5$ keV, and an X-ray-to-optical flux ratio $\log (F_X/F_V)_u = -2.14$. These properties seem to suggest an AB nature. However, according to Geller et al. (2008), the optical counterpart to this source (WOCS 5639) is a single cluster member. They note that stars classified as single may be binaries that cannot be detected as such because they have low-amplitude radial-velocity variations and/or long orbital periods. A long-period binary with main-sequence components, however, is not expected to be an X-ray source as there is little interaction between the two stars in such a system. Hence, we place CX 33 under the category of 'uncertain classification'.

3.2 Uncertain membership

Sources that do not have a membership probability based on either proper motion or radial velocity are classified as uncertain members of the cluster. We found seven such sources of which

two were detected previously by *XMM–Newton* (CX 24/GX 57 and CX 28/GX 31) and five are newly detected sources (CX 14, CX 29, CX 45, CX 48, and CX 76).

Six of the seven uncertain members are proposed as CV or AGN candidates as they lie to the blue of the cluster main sequence and have $\log (F_X/F_V)_u > -0.46$. Of these six, CX 24 has the highest possibility of being a CV, as it is also matched with the short-period variable WV 2 (Kafka & Honeycutt 2003) with a photometric period of 0.15049 d. For these sources, either confirmation of cluster membership (or non-membership) or optical spectroscopy can help establish their nature.

For the one remaining source, classification is uncertain. CX 48 is found at the lower end of the cluster main sequence and has a high value of the median energy, $E_{50} = 4.3 \pm 0.7$ keV. Also, its X-ray-to-optical flux ratio, $\log (F_X/F_V)_u \approx -0.7$, lies in the range for accreting binaries, or active M-stars. If CX 48 is at the distance of NGC 188, its X-ray luminosity is 1.4×10^{30} erg s^{-1}. This source could be an AB that underwent a flare during the *Chandra* observation. AcisExtract did not detect X-ray variability from C X48, but with only 10 counts the sensitivity for detecting variability is low.

3.3 Cluster non-members

A total of 16 sources with candidate counterparts that have $MP_{PM} = 0$ per cent or $MP_{RV} = 0$ per cent are considered to be non-members. These sources are most likely a mix of foreground stars (those with bright counterparts and soft X-ray spectra) and AGNs (with blue/faint counterparts, e.g. the X-ray variable CX 11). In case of CX 51, where MP_{PM} is 98 per cent but MP_{RV} is 0 per cent, we consider the radial-velocity information to be more constraining and hence, classify the source as a non-member. No proper motion or radial velocity has been reported for the counterpart to CX 3, but at $V = 9.5$ this star is too bright to be a cluster member.

3.4 Sources without candidate optical counterparts

For 48 sources, we do not find any candidate optical counterparts in the Platais et al. (2003) or the Stetson et al. (2004) catalogues. The detection limit ($V \approx 22$) of the Platais et al. catalogue allows us to place approximate lower limits on their X-ray-to-optical flux ratios. These limits range from $\log (F_X/F_V)_{u,lim} \approx -0.15$ for the faintest (CX 83) to $\log (F_X/F_V)_{u,lim} \approx 1.2$ for the brightest (CX 5) unmatched source. The average E_{50} for the unmatched sources is 2.2 ± 0.6 keV (versus 1.6 ± 0.8 keV for sources that do have candidate counterparts). These properties are consistent with an AGN nature, an explanation that also looks plausible when considering the number of unmatched sources. Among the 60 sources inside r_h with ≥ 5 net counts, 30 do not have any candidate optical counterparts. Given that we expect 31.2 ± 5.6 AGNs in this area with ≥ 5 counts (see Section 2.4), and that we have identified <10 candidate AGNs among the sources *with* candidate counterparts inside r_h, it is likely that the majority of the sources without an optical match are AGNs.

4 DISCUSSION

We conducted an X-ray study of the old open cluster NGC 188 using *Chandra*. Our study is several times more sensitive than observations of the cluster done with *ROSAT* (Belloni et al. 1998) and *XMM–Newton* (Gondoin 2005). Unlike in these previous studies, the *Chandra* pointing was centred on the cluster centre, providing a more symmetric coverage of the cluster. Also, the positional

accuracy of *Chandra* helps us in identifying candidate optical counterparts to the X-ray sources. Of the 84 X-ray sources detected by *Chandra*, 35 unique X-ray sources have a single candidate optical counterpart, while one X-ray source (CX 76) has at least two candidate optical counterparts. Of the remaining 48 X-ray sources, 12 appear to have candidate optical counterparts in the *V*-band image by Stetson et al. (2004), however, these faint sources are neither included in the Stetson et al. (2004) nor in the Platais et al. (2003) catalogue.

As shown by Mathieu, Meibom & Dolan (2004), late-type main-sequence binaries in NGC 188 show a transition around $P_{sp} = 15.0$ d from circular orbits (below this period) to eccentric orbits (for longer periods). This demonstrates that at 7 Gyr (i.e. the age of NGC 188) tidal interaction has had sufficient time to circularize orbits up to this cut-off period. Since tidal synchronization of the stars' rotation occurs before circularization (e.g. Zahn 1989), we expect late-type binaries with orbital periods at least up to 15 d to have achieved tidal coupling ($P_{rot} = P_{sp}$) and have enhanced levels of X-ray emission compared to single stars of similar age and mass. Indeed, all the ABs discussed in Section 3.1.1 have periods shorter than 15 d, except CX 13 for which the radial-velocity period is longer (discussed below).

The X-ray activity of a late-type main-sequence star is related to its rotation period (Pizzolato et al. 2003). Generally, the X-ray luminosity increases with decreasing rotation period and follows the relation $L_X \propto P_{rot}^{-2}$. However, for short periods a star reaches a 'saturated' regime, where L_X no longer depends on P_{rot}, but instead flattens to $L_X/L_{bol} \sim 10^{-3}$ with L_{bol} being the bolometric luminosity of the star (Randich 1998; Güdel 2004). Stars with the shortest periods appear to emit X-rays at a level even lower than predicted by this saturated luminosity relation. Such stars are said to be 'super-saturated' (Prosser et al. 1996) and this behaviour has been ascribed to either a change in the dynamo action of the star or the reduction in the area of the active regions (see section 5.4 in Güdel 2004). In Fig. 5, we plotted L_X versus a measure of P_{rot} for cluster members that were matched with a *Chandra* source to see if we observe this behaviour in NGC 188. The periods used for the sources on the top panel were taken from the radial-velocity orbital solutions from Geller et al. (2009) if available (CX 13, CX 26, CX 53, CX 84), and otherwise from variability surveys (Zhang et al. 2004; Mochejska et al. 2008). We can see that the overall behaviour of L_X as a function of period is in line with the trend described above, albeit with significant scatter. Moving from $\sim$7 d to shorter periods, L_X reaches higher values until $\sim$1.3 d; this is similar to what we see for the ABs in M 67 (van den Berg et al. 2004). For shorter periods, L_X starts diminishing again – this may correspond to the supersaturation regime. Three sources are outliers: CX 13, CX 26, and CX 84. For CX 13 and CX 84 the period from radial velocities is different from the reported photometric period. If we plot the latter instead (bottom panel), these two sources are more in line with the trend described. CX 13 and CX 84 are described in more detail in Sections 4.1 and 4.2. The SSG CX 26 is more X-ray luminous for its period compared to the overall trend; the spectroscopic period is the only measure for the rotation period available.

There are nine cluster members within the *Chandra* FOV with orbital periods from Geller et al. (2009) below $\sim$15 d, which were not detected in X-rays. Six of these sources could simply have X-ray luminosities below our detection limit as their periods are relatively long (8 d $< P_{sp} <$ 15 d). In addition, WOCS 5762 ($P_{sp} = 6.5$ d) and WOCS 5147 ($P_{sp} = 6.7$ d) are found further away from the aimpoint where the X-ray detection limit is higher. However, we cannot explain the non-detection of WOCS 5052. This spectroscopic binary
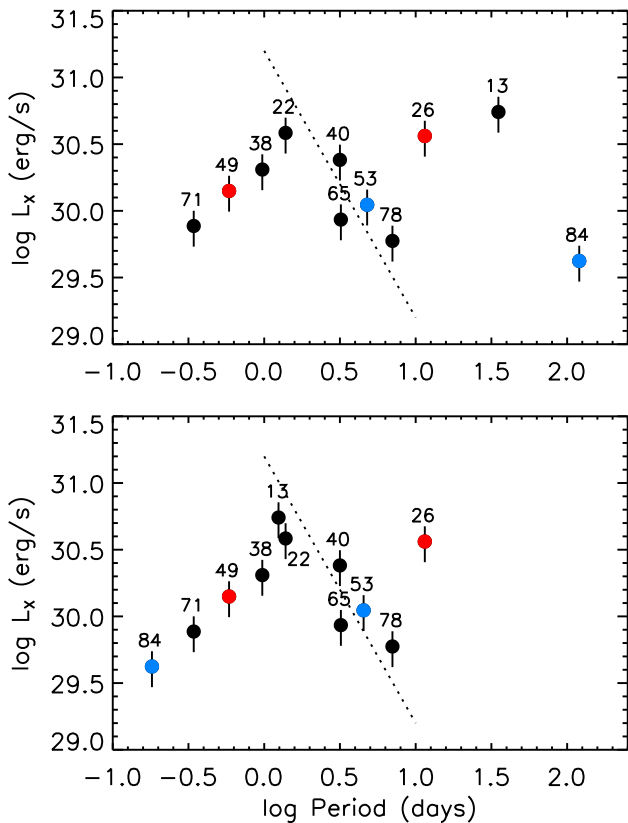
Figure 5. X-ray luminosity (L_X) versus rotation period (P_{rot}) plot, where either P_{ph} or P_{sp} is taken as a measure of P_{rot}. In the top panel, P_{rot} is based on radial velocities (P_{sp}) if available, and otherwise on variability studies. In the bottom panel, the periods are from variability studies (P_{ph}) if available, and otherwise from radial velocities. Blue stragglers are marked with blue circles, and sub-subgiants with red circles. The dashed line shows the relation $L_X \propto P_{rot}^{-2}$ with an arbitrary vertical offset; note this is *not* a fit to the data. L_X is based on fluxes computed for an assumed 2 keV MeKaL spectrum and the cluster N_H; errors on L_X stem mostly from the unknown underlying spectrum, and are of the order of up to 20–30 per cent. Error bars of 30 per cent in L_X are plotted, while the formal errors on the periods are negligible.

lies closer to the aimpoint; it has a 3.85 d spectroscopic period and a near-circular orbit ($e = 0.05 \pm 0.03$; Geller et al. 2009).

4.1 CX 13

The optical counterpart to CX 13 (WOCS 4705) is an eccentric ($e = 0.487 \pm 0.005$), double-lined spectroscopic binary with an orbital period of $P_{sp} \approx 35.2$ d (Geller et al. 2009). Its orbital parameters set this X-ray source apart from typical ABs, which have shorter orbital periods and circular orbits. Indeed, the location of this binary in the diagnostic diagrams of Verbunt & Phinney (1995, figs 5a and b) indicates the orbit is too wide for the primary to have circularized the orbit within the age of the cluster. However, since the time-scale for tidal synchronization is shorter than for circularization, the rotation of one or both stars in this binary can already be faster compared to single (sub)giants or turnoff stars in NGC 188, which would explain the X-ray emission. The pseudo-synchronization period, defined in Hut (1981) to be the spin period of the star if it corotates with the average orbital speed around periastron, is 13.1 d in this binary. This is a bit longer than the corotation period at periastron passage (10.6 d). CX 13 may be an RS CVn-like

system like the binary and X-ray source S 1242 in M 67, which is an eccentric ($e = 0.66$) $P_{sp} = 31.8$ d period binary on the subgiant branch.

WOCS 4705 is the optical variable V 11. The observed 0.4 mag drop in brightness led Kaluzny (1990) to postulate that V 11 is a possible eclipsing RS CVn binary. Interestingly, Geller et al. (2009), based on their orbital ephemeris, found that this dip in brightness occurred at the orbital phase where an eclipse would indeed be expected to occur. Subsequent variability studies (Mazur & Kaluzny 1990; Zhang et al. 2004) only observed small-amplitude variations (0.03–0.08 mag). Zhang et al. (2004) reported a possible photometric period of 1.2 d. We note that folding the published photometry for V 11 on this period does not produce a smooth light curve; on the other hand, this period does give a better match to the L_X versus P_{rot} trend in Fig. 5. If real, the origin of this period is unexplained. CX 13 lies within the core radius of the cluster, where the number of spurious matches between X-ray sources and photometric variables is expected to be ~0.013, making the chance alignment of CX 13 with a variable very unlikely.

4.2 CX 84

CX 84 is a source located 3′.7 from the cluster centre that is identified with the BSS WOCS 5379. From radial velocities Geller et al. (2009) derived an eccentric ($e = 0.24 \pm 0.03$) orbit with a period of $P_{sp} = 120.21$ d. It is one of the seven BSSs in NGC 188 for which FUV observations with the *Hubble Space Telescope* uncovered an excess flux compared to what is expected from the BSS alone, showing that the companion in these systems (all spectroscopic binaries) is a white dwarf (Gosnell et al. 2014, 2015). From the temperature of the white dwarf in WOCS 5379 ($T \approx 17\,600$ K), it was derived that it formed only ~77 ± 7 Myr ago. Gosnell et al. (2014) sketched a possible evolutionary scenario, in which the original secondary became a BSS after mass accretion from the white-dwarf progenitor. However, there are two aspects left unexplained by this evolutionary path. It fails to explain the highly eccentric orbit, as mass transfer via Roche lobe overflow should circularize the orbit of the binary quite rapidly [although under certain circumstances this is not necessarily the case, see Sepinsky et al. (2007, 2009)]. Also, the nature of the binary components does not account for the X-rays: the white dwarf is not hot enough for thermal X-ray emission, and it is not obvious why the BSS would be an X-ray source. Another cluster BSS within the *Chandra* FOV, WOCS 4540, with an age (70 ± 7 Myr; Gosnell et al. 2014) similar to WOCS 5379, was not detected as an X-ray source.

The key to solving this puzzle may lie in the optical variability that was detected for WOCS 5379. Kafka & Honeycutt (2003) found this source to be a photometric variable (WV 3) with a V amplitude of 0.22 mag and a period of $P_{ph} = 0.18148$d (if the light curve has one maximum/minimum per period), or instead $P_{ph} = 0.36296$d if there are two maxima/minima per period. What is the origin of this variability? According to Geller et al. (2009), WOCS 5379 lies outside the instability strip, ruling out pulsations as a likely explanation. Alternatively, the variability may be the signature of a short-period binary 'hiding' in the system. The distribution of the data points around photometric minimum when folded on the shorter period (Kafka & Honeycutt 2003) looks bimodal, which may be a sign that the actual period is ~0.36 d and that the two minima are uneven. The presence of a short-period binary in the system would provide possible explanations for the X-rays (coronal activity, low-level mass transfer). On the other hand, it remains unclear what the exact configuration of such a hierarchical multiple system would

be and whether any of the observed system components (the BSS and the white dwarf) are part of the short-period binary. Geller et al. (2009) report that they were unable to derive a kinematic orbital solution for a period of 0.18148d, and also do not find a sign of rapid rotation in the spectrum of WOCS 5379. This implies that the BSS, which dominates the optical spectrum, is not part of the short-period binary. The white dwarf could have a close companion, perhaps similar to the pre-cataclysmic variables. But if mass transfer from the white-dwarf progenitor to the BSS progenitor in the wide orbit ended only ∼77 Myr ago (as inferred from the cooling age of the white dwarf), then this close companion entered the system only recently (in an encounter that perhaps also induced the eccentricity), complicating this speculative formation scenario even more. An extensive exploration of conceivable evolutionary scenarios is beyond the scope of this paper. In light of our findings, which suggest that CX 84/WOCS 5379 is not a binary but a triple or higher order multiple, we conclude that its actual formation may be more complicated than the scenario of mass transfer between two binary components as sketched by Gosnell et al. (2014). In star clusters with a binary frequency exceeding 10 per cent (such as in NGC 188 where the frequency of main-sequence binaries with periods up to 10^4 d is 29 ± 3 per cent; Geller & Mathieu 2012), binary–binary encounters typically dominate over binary–single-star encounters (Sigurdsson & Phinney 1993; Leigh & Sills 2011), producing, among others, hierarchical triples. Leigh & Geller (2013) have demonstrated the significance of dynamical encounters involving triple systems, especially in open clusters. In fact, as has been argued by Leigh & Sills (2011), a considerable fraction of the blue stragglers in NGC 188 could have a dynamical origin. Such dynamical encounters can become quite complex: in low-mass star clusters such as old open clusters or low-mass globular clusters, the encounter durations are comparable to the time-scale for another encounter to happen. As a result, the probability of an ongoing encounter being interrupted by a subsequent encounter can be up to a few tens of per cent (Geller & Leigh 2015). The same is found when binaries of hydrogen-rich, non-degenerate stars undergoing stable mass transfer are considered: in low-mass clusters, the encounter time-scale is comparable to the duration of the mass-transfer phase, resulting in a significant probability that a mass-transfer binary could be disrupted or affected by other nearby stars (Leigh, Geller & Toonen 2016). The outcomes of such events, or sequence of events, are difficult to predict for individual cases, but the point is that the possibility of dynamical interactions playing a role in the formation of CX 84/WOCS 5379 should not be neglected.

We conclude that WOCS 5379 is an interesting target for follow-up studies to improve the current light-curve and period measurements. Also, high-signal-to-noise high-resolution spectra would enable a search for activity or accretion signatures. By subtracting a high-quality template spectrum for the BSS, one could look for any additional components contributing to the optical spectrum. A similar technique was used to uncover a close binary in the spectrum of the BSS S 1082 in M 67 (van den Berg et al. 2001), for which a long orbital period was found from radial velocities (∼1189 d; Sandquist et al. 2003) while at the same time eclipses on a 1 d period had been reported (Goranskij et al. 1992).

4.3 Comparison with other old star clusters

We compare the number of X-ray sources that we find in NGC 188 to those found in other old open clusters. To compare these results uniformly, we select sources brighter than $L_X \approx 1 \times 10^{30}$ erg s^{-1} (0.3–7 keV) that are found inside r_h. For NGC 188, using a 2 keV MeKaL model to estimate the X-ray fluxes, we observe 55 such sources. Of these 55 X-ray sources, 9 are confirmed cluster members, and another 3 have uncertain membership classification (the remaining ones are likely AGNs). Among these, four are ABs (CX 13, CX 22, CX 38, CX 40), two are CV/AGN candidates (CX 14, CX 28), two are SSGs (CX 26, CX 49), one is a BSS (CX 53), one an FK Com (CX 4), and two sources have uncertain classification (CX 33, CX 48). We present these numbers in Table 4, and compare them with four other old open clusters. We find that the addition of NGC 188 to the sample confirms the trend that the number of X-ray sources appears to scale with mass in open clusters when the three clusters with the highest quality membership information (M 67, NGC 188, and NGC 6791) are considered. This is expected for a population that is (mostly) of primordial origin. The number of ABs does not show an obvious scaling with mass; the small source samples inhibit making any firm conclusions.

It has been pointed out that globular clusters and other old stellar populations appear to be deficient in X-ray luminosity per unit mass, when compared to old open clusters (e.g. Verbunt 2000; van den Berg et al. 2013; Ge et al. 2015). X-ray emissivities of various old populations have been reported in the recent literature. Due to the variety of methods and energy bands adopted, it is not straightforward to compare the resulting values directly. The X-ray emissivities in Ge et al. (2015) were computed in a consistent manner. To enable a comparison of our result for NGC 188 with their set of X-ray emissivities of dwarf ellipticals and globular clusters, we have converted the X-ray emissivity of NGC 188 to the 0.5–2 and 2–8 keV bands for the assumption of a 2 keV MeKaL model. We find that $L_X/M \approx 15.9 \times 10^{27}$ erg s^{-1} M$_\odot^{-1}$ (0.5–2 keV), which is indeed higher than the X-ray emissivities in Table 2 from Ge et al. However, in the 2–8 keV band, the extrapolated NGC 188 emissivity is $L_X/M \approx 8.7 \times 10^{27}$ erg s^{-1} M$_\odot^{-1}$, which is included in the range of X-ray emissivities in Ge et al. (2015). We caution that our adopted spectral model to compute X-ray fluxes is different than the one in their paper, which is a thermal model with a log-normal temperature distribution around a (fitted) peak temperature value. A uniform reanalysis of the X-ray data of old populations lies outside the scope of this paper, but we refer the reader to the forthcoming paper by Heinke et al. that makes an in-depth comparison of X-ray emissivities of globular clusters and those of other old stellar populations, including old open clusters.

We illustrate the elevated X-ray emission of old open clusters with concrete numbers. NGC 188 has a mass of 2600 ± 460 M$_\odot$ (Geller et al. 2008) and has two members (the FK Com star CX 4 and the subgiant AB CX 13) with $L_X \gtrsim 5 \times 10^{30}$ erg s^{-1} (0.3–7 keV) within r_h. In M 67, with a mass of 2100^{+610}_{-550} M$_\odot$ (Geller, Latham & Mathieu 2015) there are three members above this luminosity limit: an SSG, a BSS, and an AB. Finally, in NGC 6791 (5000–7000 M$_\odot$; Platais et al. 2011), seven to eight members are detected above this luminosity limit; they are a mix of CVs, SSGs, ABs, and an apparently single red giant. In contrast, the two sparse globular clusters Terzan 3 and NGC 6535 with masses ∼12 000 M$_\odot$ were also observed down to ∼5 × 10^{30} erg s^{-1} (0.3–7 keV) with *Chandra*, and zero sources were detected inside r_h (A. Kong, private communication). Several factors can contribute to the enhanced X-ray emissivity of old open clusters, including the faster rate at which stars are lost from open clusters compared to globular clusters as a result of their shorter relaxation times (reducing their mass more severely), the higher rate of dynamical destruction in globular clusters of certain types of binaries that contribute to the X-ray source

Table 4. Comparison of X-ray sources in old open clusters with $L_X \geq 10^{30}$ erg s^{-1} (0.3–7 keV) inside r_h.

Cluster	Age (Gyr)	Mass (M$_\odot$)	N_X	$N_{X,CV}$	$N_{X,SSG}$	$N_{X,AB}$	log($2L_{30}$/Mass)
M 67[1]	4	2100^{+610}_{-550}	12	0	1	7–8	28.6
NGC 188[2]	7	2300 ± 460	9–12	≤ 2	2	4	28.4–28.5
NGC 6819[3]	2–2.4	2600	3–8	$\lesssim 1$	$\lesssim 1$	$\lesssim 4$	28.8–29.3
NGC 6791[4]	8	5000–7000	15–19	3–4	3	7–11	28.6–28.8
Cr 261[5, a]	7	5800–7200	$\lesssim 26 \pm 8$	$\lesssim 4$	$\lesssim 2$	2–23	$\lesssim$28.6–28.7

Notes. Col. (1): Cluster name.
Col. (2): Cluster age in Gyr.
Col. (3): Mass of the cluster in M$_\odot$.
Col. (4): The number of X-ray sources within $r \leq r_h$ and $L_X \geq 1 \times 10^{30}$ erg s^{-1}.
Col. (5): The number of CVs within aforementioned radius and luminosity limit.
Col. (6): The number of SSGs within aforementioned radius and luminosity limit.
Col. (7): The number of ABs within aforementioned radius and luminosity limit.
Col. (7): Ratio of the total X-ray luminosity of sources inside r_h brighter than 1×10^{30} erg s^{-1} (L_{30}), and cluster mass. The multiplicative factor 2 is included to scale the mass estimate to the half-mass radius.
References – [1]van den Berg et al. (2004); Geller et al. (2015), [2]this work and Chumak et al. (2010), [3]Gosnell et al. (2012); Platais et al. (2013), [4]van den Berg et al. (2013); Platais et al. (2011), [5]Vats & van den Berg (2017).
[a]Membership information is unavailable for Cr 261, leading to large uncertainties.

populations of open clusters, differences in age, and differences in metallicity (see also the discussion in section 5.2 of Vats & van den Berg 2017). Further studies of more clusters with a range of properties are needed to gain more insight.

5 SUMMARY

We present the results of a new X-ray study of the 7 Gyr old open cluster NGC 188. *Chandra* detected 84 sources above $L_X \approx 4 \times 10^{29}$ erg s^{-1} (0.3–7 keV), of which 73 lie within the half-mass radius. Of the thirteen cluster members that were detected by *Chandra*, seven are new X-ray detections. The X-ray source population of this cluster is a mix of ABs, SSGs, BSSs, and a single FK Com star. While some of these X-ray source types are frequently seen in other old open clusters, we also found a few surprises. CX 33 is an apparently single cluster star on the main sequence, and we do not understand its X-ray emission. CX 13 (V 11) is an AB that may be on its way to being circularized. The orbital parameters of the BSS and white-dwarf binary WOCS 5379 already were puzzling given the combination of an eccentric orbit in a post-mass-transfer system, but the detection of X-rays (CX 84) makes this system even more intriguing. It raises the question whether the short-period variability that has been reported for this star is coming from a close binary inside the system, which would also explain the X-ray emission. Considering the overall X-ray population in NGC 188, we confirm our findings that the X-ray emissivity of old open clusters is elevated compared to other old stellar populations.

ACKNOWLEDGEMENTS

REFERENCES

Belloni T., Verbunt F., Schmitt J. H. M. M., 1993, A&A, 269, 175
Belloni T., Verbunt F., Mathieu R. D., 1998, A&A, 339, 431
Bressan A., Marigo P., Girardi L., Salasnich B., Dal Cero C., Rubele S., Nanni A., 2012, MNRAS, 427, 127
Broos P. S., Townsley L. K., Feigelson E. D., Getman K. V., Bauer F. E., Garmire G. P., 2010, ApJ, 714, 1582
Chen Y., Girardi L., Bressan A., Marigo P., Barbieri M., Kong X., 2014, MNRAS, 444, 2525
Chen Y., Bressan A., Girardi L., Marigo P., Kong X., Lanza A., 2015, MNRAS, 452, 1068
Chumak Y. O., Platais I., McLaughlin D. E., Rastorguev A. S., Chumak O. V., 2010, MNRAS, 402, 1841
Davies M. B., 2015, Formation Channels for Blue Straggler Stars, Ecology of Blue Straggler Stars, Astrophysics and Space Science Library, Vol 413. Springer-Verlag, Berlin Heidelberg, p. 203
Drimmel R., Cabrera-Lavers A., López-Corredoira M., 2003, A&A, 409, 205
Garmire G. P., Bautz M. W., Ford P. G., Nousek J. A., Ricker G. R., 2003, in Joachim E. T., Harvey D. T., eds, Proc. SPIE Conf. Ser. Vol. 4851, X-Ray and Gamma-Ray Telescopes and Instruments for Astronomy. SPIE, Bellingham, p. 28
Ge C. et al., 2015, ApJ, 812, 130
Geller A. M., Leigh N. W. C., 2015, ApJ, 808, L25
Geller A. M., Mathieu R. D., 2011, Nature, 478, 356
Geller A. M., Mathieu R. D., 2012, AJ, 144, 54
Geller A. M., Mathieu R. D., Harris H. C., McClure R. D., 2008, AJ, 135, 2264
Geller A. M., Mathieu R. D., Harris H. C., McClure R. D., 2009, AJ, 137, 3743
Geller A. M., Latham D. W., Mathieu R. D., 2015, AJ, 150, 97
Geller A. M. et al., 2017, ApJ, 840, 66
Giardino G., Pillitteri I., Favata F., Micela G., 2008, A&A, 490, 113
Gondoin P., 2005, A&A, 438, 291
Goranskij V. P., Kusakin A. V., Mironov A. V., Moshkaljov V. G., Pastukhova E. N., 1992, Astron. Astrophys. Trans., 2, 201
Gosnell N. M., Pooley D., Geller A. M., Kalirai J., Mathieu R. D., Frinchaboy P., Ramirez-Ruiz E., 2012, ApJ, 745, 57
Gosnell N. M., Mathieu R. D., Geller A. M., Sills A., Leigh N., Knigge C., 2014, ApJ, 783, L8
Gosnell N. M., Mathieu R. D., Geller A. M., Sills A., Leigh N., Knigge C., 2015, ApJ, 814, 163
Güdel M., 2004, A&AR, 12, 71

Harris H. C., McClure R. D., 1985, PASP, 97, 261

Hoffmeister C., 1964, Inf. Bull. Var. Stars, 67

Hong J., Schlegel E. M., Grindlay J. E., 2004, ApJ, 614, 508

Hong J., van den Berg M., Schlegel E. M., Grindlay J. E., Koenig X., Laycock S., Zhao P., 2005, ApJ, 635, 907

Hut P., 1981, A&A, 99, 126

Kafka S., Honeycutt R. K., 2003, AJ, 126, 276

Kaluzny J., 1990, Acta Astron., 40, 61

Kaluzny J., Shara M. M., 1987, ApJ, 314, 585

Kim M., Wilkes B. J., Kim D.-W., Green P. J., Barkhouse W. A., Lee M. G., Silverman J. D., Tananbaum H. D., 2007, ApJ, 659, 29

Leigh N., Geller A., 2013, MNRAS, 432, 2474

Leigh N., Sills A., 2011, MNRAS, 410, 2370

Leigh N., Geller A., Toonen S., 2016, ApJ, 818, 21

Mathieu R. D., Meibom S., Dolan C. J., 2004, ApJ, 602, L121

Mazur B., Kaluzny J., 1990, Acta Astron., 40, 361

Mochejska B. J. et al., 2008, Acta Astron., 58, 263

Pallavicini R., 1989, A&AR, 1, 177

Peres G., Orlando S., Reale F., Rosner R., Hudson H., 2000, ApJ, 528, 537

Pizzolato N., Maggio A., Micela G., Sciortino S., Ventura P., 2003, A&A, 397, 147

Platais I., Kozhurina-Platais V., Mathieu R. D., Girard T. M., van Altena W. F., 2003, AJ, 126, 2922

Platais I., Cudworth K. M., Kozhurina-Platais V., McLaughlin D. E., Meibom S., Veillet C., 2011, ApJ, 733, L1

Platais I., Gosnell N. M., Meibom S., Kozhurina-Platais V., Bellini A., Veillet C., Burkhead M. S., 2013, AJ, 146, 43

Predehl P., Schmitt J. H. M. M., 1995, A&A, 293, 889

Prosser C. F., Randich S., Stauffer J. R., Schmitt J. H. M. M., Simon T., 1996, AJ, 112, 1570

Randich S., 1998, in Donahue R. A., Bookbinder J. A., eds, ASP Conf. Ser. Vol. 154, Cool Stars, Stellar Systems, and the Sun. Astron. Soc. Pac., San Francisco, p. 501

Rosen S. R. et al., 2016, A&A, 590, A1

Rucinski S. M., 1994, PASP, 106, 462

Sandage A. R., 1953, AJ, 58, 61

Sandquist E. L., Latham D. W., Shetrone M. D., Milone A. A. E., 2003, AJ, 125, 810

Sarajedini A., von Hippel T., Kozhurina-Platais V., Demarque P., 1999, AJ, 118, 2894

Sepinsky J. F., Willems B., Kalogera V., Rasio F. A., 2007, ApJ, 667, 1170

Sepinsky J. F., Willems B., Kalogera V., Rasio F. A., 2009, ApJ, 702, 1387

Sigurdsson S., Phinney E. S., 1993, ApJ, 415, 631

Skumanich A., 1972, ApJ, 171, 565

Stetson P. B., McClure R. D., VandenBerg D. A., 2004, PASP, 116, 1012

Stocke J. T., Morris S. L., Gioia I. M., Maccacaro T., Schild R., Wolter A., Fleming T. A., Henry J. P., 1991, ApJS, 76, 813

Tang J., Bressan A., Rosenfield P., Slemer A., Marigo P., Girardi L., Bianchi L., 2014, MNRAS, 445, 4287

van den Berg M., Orosz J., Verbunt F., Stassun K., 2001, A&A, 375, 375

van den Berg M., Tagliaferri G., Belloni T., Verbunt F., 2004, A&A, 418, 509

van den Berg M., Verbunt F., Tagliaferri G., Belloni T., Bedin L. R., Platais I., 2013, ApJ, 770, 98

Vats S., van den Berg M., 2017, ApJ, 837, 130

Verbunt F., 2000, in Pallavicini R., Micela G., Sciortino S., eds, ASP Conf. Ser. Vol. 198, Stellar Clusters and Associations: Convection, Rotation, and Dynamos. Astron. Soc. Pac., San Francisco, p. 421

Verbunt F., Phinney E. S., 1995, A&A, 296, 709

Zacharias N., Finch C. T., Girard T. M., Henden A., Bartlett J. L., Monet D. G., Zacharias M. I., 2013, AJ, 145, 44

Zahn J.-P., 1989, A&A, 220, 112

Zhang X. B., Deng L., Zhou X., Xin Y., 2004, MNRAS, 355, 1369

This paper has been typeset from a TEX/LATEX file prepared by the author.